AIChE

Revisiting Johnson and Jackson Boundary Conditions for Granular Flows

Tingwen Li
National Energy Technology Laboratory, Department of Energy, Morgantown, WV 26505

URS Corporation, Morgantown, WV 26505

Sofiane Benyahia
National Energy Technology Laboratory, Department of Energy, Morgantown, WV 26505

DOI 10.1002/aic.12728
Published online August 2, 2011 in Wiley Online Library (wileyonlinelibrary.com).

In this article, we revisit Johnson and Jackson boundary conditions for granular flows. The oblique collision between a particle and a flat wall is analyzed by adopting the classic rigid-body theory and a more realistic semianalytical model. Based on the kinetic granular theory, the input parameter for the partial-slip boundary conditions, specularity coefficient, which is not measurable in experiments, is then interpreted as a function of the particle-wall restitution coefficient, the frictional coefficient, and the normalized slip velocity at the wall. An analytical expression for the specularity coefficient is suggested for a flat, frictional surface with a low frictional coefficient. The procedure for determining the specularity coefficient for a more general problem is outlined, and a working approximation is provided. Published 2011 American Institute of Chemical Engineers 58: 2058–2068, 2012
Keywords: granular flow, boundary condition, two-fluid model, rigid-body theory, specularity coefficient

Introduction

Gas-solids flows are involved in numerous industrial processes, including energy production and chemical, pharmaceutical, food, and agricultural processing. To optimize the design and operation of industrial processes, a thorough understanding of associated gas-solids flows is needed. With the fast development of high-speed computers and computational algorithms, computational fluid dynamics (CFD) modeling has become an important tool to help achieve this goal.

The Eulerian-Eulerian model, also known as two-fluid model, has been widely used to simulate gas-solids flows in various systems. In the Eulerian-Eulerian approach, each phase is treated as an interpenetrating continuum. The conservation equations of mass, momentum, and energy for both the particulate and the fluid phases are derived. So far, the governing equations for the solids phase are mostly closed by the kinetic granular theory, which assumes that the random motion of particles is analogous to the motion of molecules in a gas.[1] A granular temperature proportional to the mean square of the random particle velocity is then defined to model the fluctuating energy of the solids phase. Validity of the constitutive correlations based on the kinetic granular theory has been generally accepted. In addition to the valid constitutive closures, appropriate boundary conditions are crucial to the quantitative prediction of granular flows.

Correspondence concerning this article should be addressed to T. Li at tingwen.li@ur.netl.doe.gov.

Published 2011 American Institute of Chemical Engineers. This article is a U.S. Government work, and, as such, is in the public domain in the United States of America.

Boundary conditions for the granular flows of smooth, frictionless disks, and spheres have been derived for a bumpy wall composed of attached disks and spheres.[2–4] However, friction, one important factor affecting the transfer of momentum and energy at boundaries, was ignored in these boundary conditions. Jenkins[5] derived boundary conditions at a flat, frictional wall based on a model of collision that distinguishes between sticking and sliding collisions. By using a simple velocity distribution function to integrate the impulse and change in fluctuation energy over all possible collisions, he calculated the analytical expressions for the collisional exchange of momentum and fluctuation energy between particles and a wall in two asymptotic circumstances—the small-friction/all-sliding limit and the large-friction/no-sliding limit. Jenkins and Louge[6] lately improved those boundary conditions by refining the calculation of flux of fluctuation energy at the wall. It was suggested that the appropriate boundary conditions could be found by interpolating between two limits. Jenkins[7] further outlined the derivation of boundary conditions for granular flows of frictional spheres at a bumpy, frictional wall with either cylindrical or spherical bumps. Xu[8,9] then extended the boundary conditions for a frictional, bumpy boundary over a large range of slip velocities and gave the analytical expressions for two-dimensional disk flows. In these boundary conditions, material properties, including the coefficient of friction and the normal and tangential particle-wall restitution coefficients, are needed. However, these data are not abundant in the literature, especially for the tangential particle-wall restitution coefficient based on the precollision and postcollision velocities at the contact point. The tangential restitution

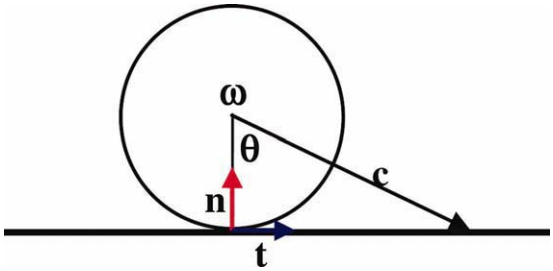

Figure 1. Schematic of particle-wall collision.

[Color figure can be viewed in the online issue, which is available at wileyonlinelibrary.com.]

coefficient referring to the motion of the center of the sphere reported in most measurements cannot be directly used for the boundary conditions.[10–12] In addition, it is not straightforward to interpolate between the two limits given by Jenkins.[13]

Johnson and Jackson[14] incorporated friction into the boundary conditions in a heuristic way by considering a boundary at which some particles collide and the rest slide. The momentum and energy transfer due to the colliding particles was characterized by a coefficient of specularity, and that of the sliding particles was depicted by Coulomb friction. This boundary condition has been widely applied in numerical simulations of gas-solids flows due to its relatively simple form. In Johnson and Jackson boundary conditions, the specularity coefficient must be specified to characterize the tangential momentum transfer due to collisions, for which the directly experimental measurement is not feasible.[15] Different specularity coefficients have been adopted in the literature with high values (~ 0.5) most common in simulating bubbling fluidized beds, whereas low values were applied to circulating fluidized bed simulations.[16] It has been demonstrated that the flow field is very sensitive to the choice of specularity coefficient.[13,16–19] Choosing the right number is critical for most validation studies as the wall effect is believed to be more important for small-scale laboratory systems than large-scale industrial plants. One way to specify the specularity coefficient is to adjust this parameter to fit some experimental data. However, this is unlikely to be feasible for large-scale fluidized bed simulations where

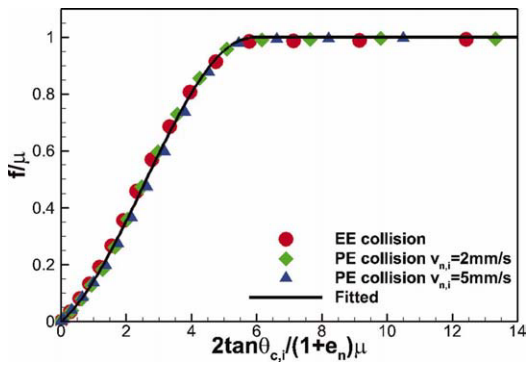

Figure 2. Numerical data on variation of f/μ with the normalized impact angle from Wu et al. (2009) for EE and PE collisions and the fitted curve by Eq. 21.

[Color figure can be viewed in the online issue, which is available at wileyonlinelibrary.com.]

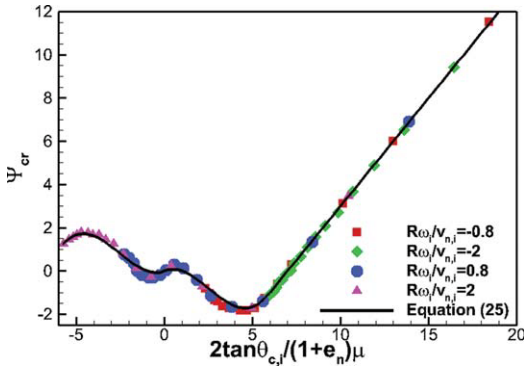

Figure 3. Variation of the non-dimensional rebound tangential surface velocity at contact patch with the normalized impact angle for oblique particle-wall contact with different initial particle spins ($c_{n,i}$ = 0.5 m/s, ν =0.3, μ =0.35, and e_n =1).

[Color figure can be viewed in the online issue, which is available at wileyonlinelibrary.com.]

the experimental measurements tend to be very limited and the computation is highly time-consuming.

A recent numerical study of gas mixing in a tall narrow fluidized bed operated under the slugging fluidization regime indicated that the specularity coefficient might be affected by the superficial gas velocity, in addition to particle and wall properties,[17] suggesting that the specularity coefficient

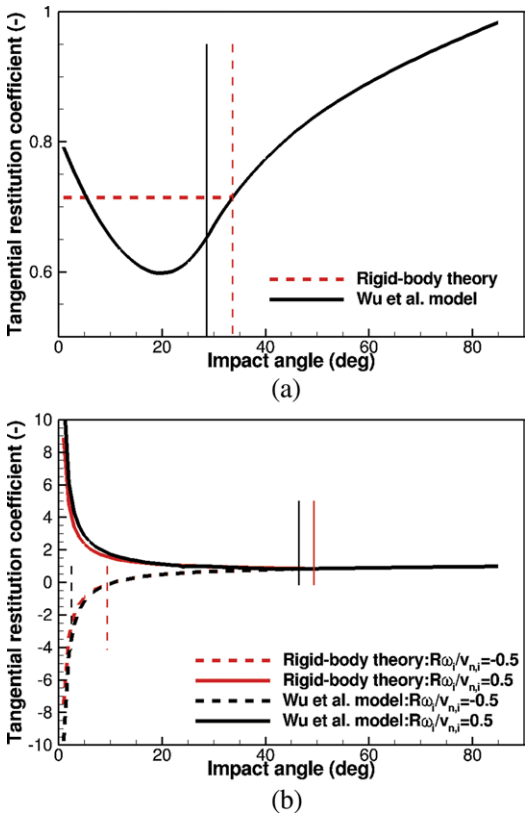

Figure 4. Variation of the tangential restitution coefficient with the impact angle (a) without initial spin, (b) with initial spin. (Vertical lines indicate transition between sliding and non-sliding collisions).

[Color figure can be viewed in the online issue, which is available at wileyonlinelibrary.com.]

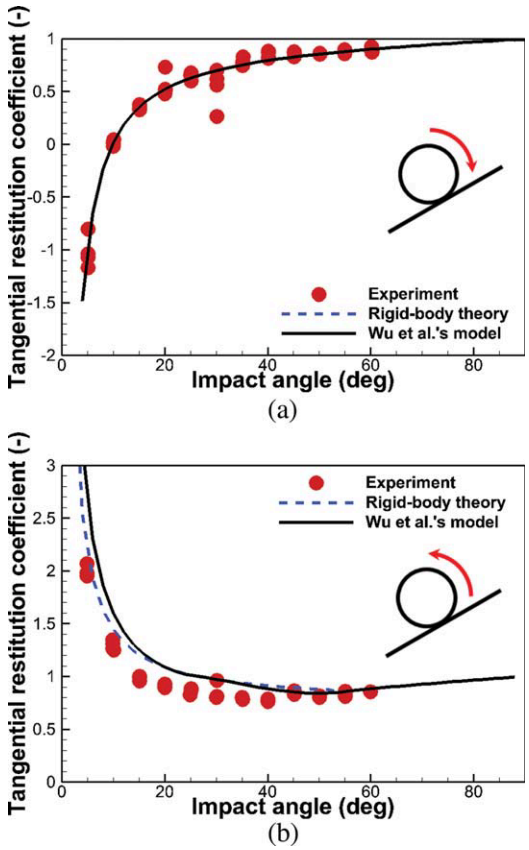

Figure 5. Variation of the tangential restitution coefficient with the impact angles for sphere-on-flat collisions with an initial spin of 80 rad/s in different directions (a) forward initial spin, (b) backward initial spin.

Note that in regions where the dashed line lies beneath the solid line, it becomes invisible. [Color figure can be viewed in the online issue, which is available at wileyonlinelibrary.com.]

fitted with certain experimental data may not work universally for the same system under different flow conditions. In that study, a lower value of specularity coefficient for Johnson and Jackson boundary conditions tends to yield the better agreement between numerical prediction and experimental data as the superficial gas velocity increased. In-depth study is required to clarify the relationship between specularity coefficient and flow conditions, wall roughness, and particle shape.

In this article, we will discuss some limitations of specularity coefficient in modeling interactions between the granular flow and the frictional wall. However, considering the wide applications of Johnson and Jackson boundary conditions in CFD codes, we try to derive expressions for the specularity coefficient based on physical analysis of particle-wall collisions. We first analyze the single particle-wall collision with the classic rigid-body theory and a recent semianalytical model. Expressions for the tangential restitution coefficient are derived accordingly. On the basis of these analyses, we revisit Johnson and Jackson boundary conditions for granular flows and develop a model to determine the specularity coefficient for a flat, frictional wall.

Particle-wall collision

In derivation of the wall boundary conditions for granular flows, the momentum and energy fluxes are calculated by summing up the change in momentum and energy in a single collision between a sphere and the boundary over all possible collisions.[5,15] Hence, it is natural to start with the collision between a single sphere and a flat surface.

During the collision between a spherical particle and a stationary rigid wall as schematically shown in Figure 1, the wall exerts an impulse $\mathbf{J}$ to the sphere. Before the collision, the sphere has translational velocity $\mathbf{c}_i$, angular velocity $\boldsymbol{\omega}_i$, and an impact angle of θ_i. The corresponding postcollision velocities are $\mathbf{c}_r$ and $\boldsymbol{\omega}_r$. The velocities before and after collision are related by

$$m(\mathbf{c}_r - \mathbf{c}_i) = \mathbf{J} \tag{1}$$

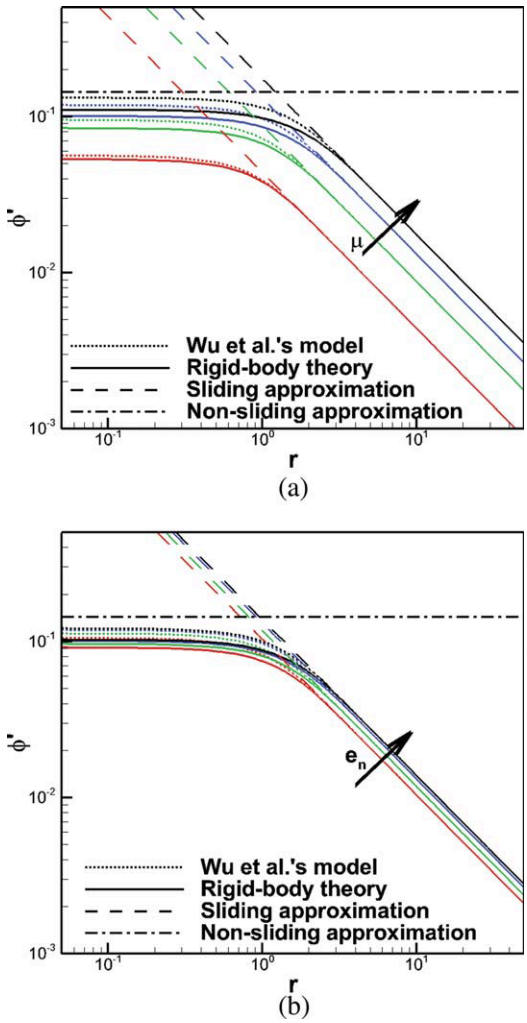

Figure 6. Variation of the effective specularity coefficient predicted by different models (a) effect of the frictional coefficient, e_n=0.9, μ=0.1, 0.2, 0.3, and 0.4; (b) effect of the normal particle-wall restitution coefficient, μ=0.3, e_n=0.5, 0.7, 0.9, and 1.0.

[Color figure can be viewed in the online issue, which is available at wileyonlinelibrary.com.]

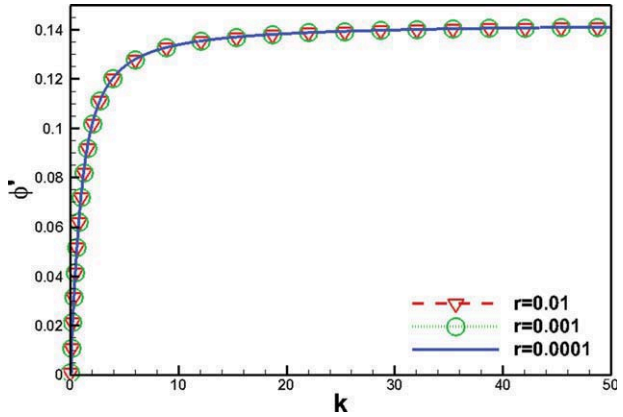

Figure 7. Variation of the effective specularity coefficient with *k* for small values of *r* (numerical integration based on the rigid-body theory).

[Color figure can be viewed in the online issue, which is available at wileyonlinelibrary. com.]

$$\frac{I(\boldsymbol{\omega}_\mathbf{r}-\boldsymbol{\omega}_\mathbf{i})}{R}=-\mathbf{n}\times\mathbf{J}-\mathbf{M}_\mathbf{r} \tag{2}$$

where $\mathbf{n}$ is the normal vector of wall, $I=2mR^2/5$ is the moment of inertia of the sphere, m is the mass of the spherical particle, R is the radius of the sphere, and $\mathbf{M}_\mathbf{r}$ comes from the rolling friction.[20] In the following analyses, we neglect the effect of rolling friction to simplify the analysis as the influence of rolling resistance on the impact properties of a sphere is negligible.[21]

The normal and tangential translational velocities before and after collision are written as

$$\mathbf{c}_{\mathbf{n},\mathbf{i}}=(\mathbf{c}_\mathbf{i}\cdot\mathbf{n})\mathbf{n} \tag{3}$$

$$\mathbf{c}_{\mathbf{t},\mathbf{i}}=\mathbf{c}_\mathbf{i}-\mathbf{c}_{\mathbf{n},\mathbf{i}} \tag{4}$$

$$\mathbf{c}_{\mathbf{n},\mathbf{r}}=(\mathbf{c}_\mathbf{r}\cdot\mathbf{n})\mathbf{n} \tag{5}$$

$$\mathbf{c}_{\mathbf{t},\mathbf{r}}=\mathbf{c}_\mathbf{r}-\mathbf{c}_{\mathbf{n},\mathbf{r}} \tag{6}$$

with subscripts $\mathbf{n}$ and $\mathbf{t}$ standing for normal and tangential components, and $\mathbf{i}$ and $\mathbf{r}$ denoting the incident and rebound velocities. The precollision and postcollision velocities at the contact point are

$$\tilde{\mathbf{c}}_\mathbf{i}=\mathbf{c}_\mathbf{i}-R\boldsymbol{\omega}_\mathbf{i}\times\mathbf{n} \tag{7}$$

$$\tilde{\mathbf{c}}_\mathbf{r}=\mathbf{c}_\mathbf{r}-R\boldsymbol{\omega}_\mathbf{r}\times\mathbf{n} \tag{8}$$

Introducing the normal and tangential impulses, $\mathbf{J}_\mathbf{n}$ and $\mathbf{J}_\mathbf{t}$, Eqs. 1 and 2 can be rewritten as

$$m\left(\mathbf{c}_{\mathbf{n},\mathbf{r}}-\mathbf{c}_{\mathbf{n},\mathbf{i}}\right)=\mathbf{J}_\mathbf{n} \tag{9}$$

$$m\left(\mathbf{c}_{\mathbf{t},\mathbf{r}}-\mathbf{c}_{\mathbf{t},\mathbf{i}}\right)=\mathbf{J}_\mathbf{t} \tag{10}$$

$$\frac{I(\boldsymbol{\omega}_\mathbf{r}-\boldsymbol{\omega}_\mathbf{i})}{R}=-\mathbf{n}\times\mathbf{J}_\mathbf{t} \tag{11}$$

In the literature, the following parameters are usually defined to characterize an oblique collision.

$$e_\mathrm{n}=-\mathbf{c}_{\mathbf{n},\mathbf{r}}/\mathbf{c}_{\mathbf{n},\mathbf{i}} \tag{12}$$

$$e_\mathrm{t}=\mathbf{c}_{\mathbf{t},\mathbf{r}}/\mathbf{c}_{\mathbf{t},\mathbf{i}} \tag{13}$$

$$f=|\mathbf{J}_\mathbf{t}|/|\mathbf{J}_\mathbf{n}| \tag{14}$$

where e_n, e_t, and f are the normal and tangential restitution coefficients and the impulse ratio, respectively. The velocity at the center of mass is used to define the restitution coefficients for both normal and tangential directions. Hence, e_n and e_t can be used to measure the recovery of translational kinetic energy in normal and tangential directions after the collision. It should be noted that the restitution coefficients defined here are different from those defined in some experimental measurements[22] which were based on the precollision and postcollision velocities at the contact point.

Generally, both normal and tangential restitution coefficients are affected by the initial velocity and the impact angle. For example, the normal restitution coefficient decreases with the increase of impact velocity.[23,24] However, it is usually safe to assume the normal restitution coefficient constant, given the range of impact velocity is not too wide. This assumption is used in the following analysis to derive the tangential restitution coefficient based on the classical rigid-body theory, many aspects of which have been shown valid for practical impacts with small elastic deformations.[10]

Rigid-body Theory

The rigid-body analysis is based on the concepts of impulse and momentum and excludes details of the transient forces and deformation occurring during the collision. According to the rigid-body theory, only two possible rebound behaviors correspond to sliding and non-sliding collision processes for a rigid spherical body colliding with the wall. For a nonsliding collision, relative displacement of the contact point does not occur so that the sphere is rolling on the surface during the contact, that is, $\tilde{\mathbf{c}}_\mathrm{r}=0$. The condition for a nonsliding collision is given as[25]

$$\left|\tilde{\mathbf{c}}_{\mathbf{t},\mathbf{i}}\right|\le\frac{7}{2}\mu(1+e_n)\left|\mathbf{c}_{\mathbf{n},\mathbf{i}}\right| \tag{15}$$

where μ is the coefficient of friction. The postcollision velocities can be calculated as

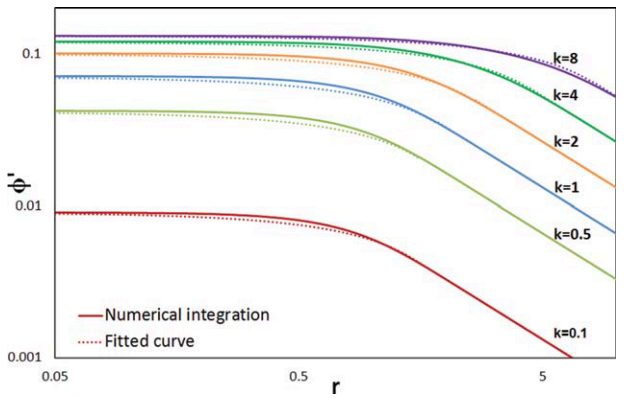

Figure 8. Variation of the effective specularity coefficient predicted by the rigid-body theory for different values of *k*.

[Color figure can be viewed in the online issue, which is available at wileyonlinelibrary.com.]

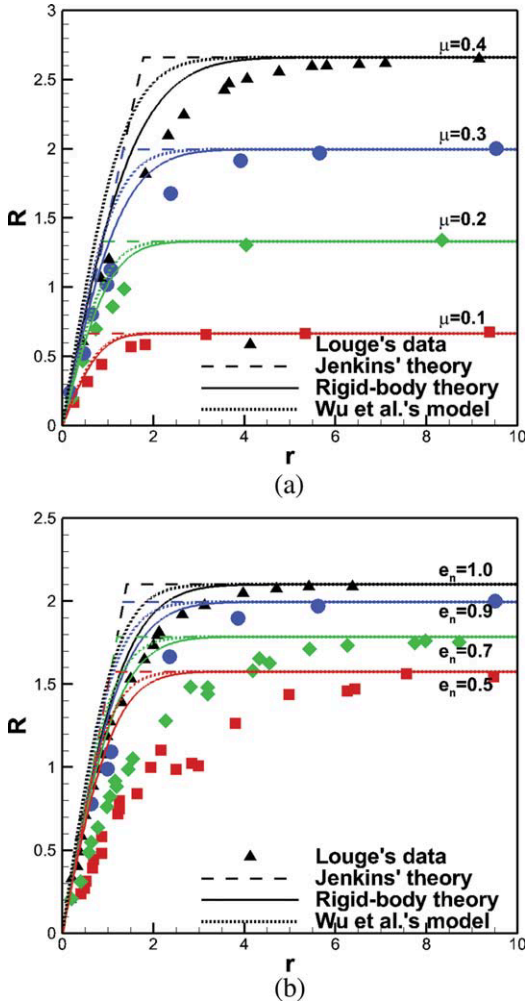

Figure 9. Variation of $R = \frac{7}{2}\frac{1+e_n}{1+\beta_0}\frac{S}{N}$ with r. (a) $e_n = 0.9$, $\beta_0 = 0$ (b) $\mu = 0.3$, $\beta_0 = 0$. (Symbols are numerical data of particle simulations from Louge 1994[35]).

[Color figure can be viewed in the online issue, which is available at wileyonlinelibrary.com.]

$$\mathbf{c}_{t,r} = \frac{5}{7}\mathbf{c}_{t,i} + \frac{2}{7}R\boldsymbol{\omega}_i \times \mathbf{n} \tag{16}$$

$$\boldsymbol{\omega}_r = \frac{5}{7R}\mathbf{n} \times \mathbf{c}_{t,i} + \frac{2}{7}\boldsymbol{\omega}_i \tag{17}$$

Clearly, the tangential restitution coefficient is dependent on the initial spin for a nonsliding collision.

The sliding collision is described by Coulomb friction theory, that is, $f = \mu$. Hence, it can be derived from Eqs. 9–11 that

$$\mathbf{c}_{t,r} = \mathbf{c}_{t,i} - \mu(1+e_n)\left|\mathbf{c}_{n,i}\right|\frac{\tilde{\mathbf{c}}_{t,i}}{\left|\tilde{\mathbf{c}}_{t,i}\right|} \tag{18}$$

$$\boldsymbol{\omega}_r = \boldsymbol{\omega}_i + \frac{5}{2R}\mu(1+e_n)\left|\mathbf{c}_{n,i}\right|\mathbf{n} \times \frac{\tilde{\mathbf{c}}_{t,i}}{\left|\tilde{\mathbf{c}}_{t,i}\right|} \tag{19}$$

In the following discussion, we assume $\boldsymbol{\omega} \times (\mathbf{n} \times \mathbf{t}) = 0$ to simplify the analyses. With this assumption, the movement of the particle center of mass is confined in a plane normal to the wall. By choosing a right-handed coordinate with **n**, **t**, and **ω**, the tangential restitution coefficient can be obtained based on Eqs. 16 and 18.

$$e_t = \begin{cases} \frac{5}{7} + \frac{2}{7}\frac{R\omega_i}{c_{t,i}} & \left|c_{t,i} - R\omega_i\right| \le \frac{7}{2}\mu(1+e_n)c_{n,i} \\ 1 - \text{sign}(c_{t,i} - R\omega_i)\mu(1+e_n)\cot\theta_i & \text{otherwise} \end{cases} \tag{20}$$

The tangential restitution coefficient predicted by the rigid-body theory works reasonably well for the sliding collision but is unable to capture the rolling collision for sphere-on-flat collisions with small impact angles.[10,11,26] This is because the rigid body analysis fails to include the material properties, the contact deformation, and the tangential, elastic compliance of the contact surfaces.[10]

Model of Wu et al.

Oblique collisions usually involve plastic deformation and microslip at the contact surfaces. The associated complicated mechanics at the microscale makes predictions of appropriate macroscopic collision characteristics difficult. Numerous attempts have been reported to include complex contact mechanics. Maw et al.[24,25] developed a solution for the oblique impact of an elastic sphere on a half-space following Hertz theory. They showed, both theoretically and experimentally, that the tangential elastic compliance of the contact surfaces due to friction significantly affected the rebound kinematics for nonsliding collisions. Based on a linear model of the contact mechanics, Di Maio and Di Renzo[27] developed an analytical solution for the oblique frictional-elastic impact of two particles and of one particle with a flat wall. Kruggel-Emden et al.[28] further extended the analytical solution of a spherical particle with a wall in the framework of a linear viscoelastic normal and a frictional-elastic tangential model. A semianalytical model for oblique impacts of elasto-plastic spheres was developed by Wu et al.[26] to predict the rebound kinematics based on finite element analysis (FEA).

Here, we follow the semianalytical model by Wu et al.[26] to further the study on oblique particle-wall impacts. In model of Wu et al., oblique collisions were classified into two regimes, namely, persistent sliding collision and nonpersistent sliding collision, which are similar to the sliding and nonsliding collisions in the rigid-body analysis. For both regimes, expressions for the variation of impulse ratio with incidence angle were derived. Specifically, it was demonstrated that for a nonpersistent sliding collision, the rebound kinematics depend on Poisson's ratio and the normal restitution coefficient. An empirical correlation in the form of hyperbolic function with four parameters was used to fit the numerical data, which presents good accuracy and robustness in comparison to FEA results and experimental data published in the literature.[26] For a Poisson's ratio of 0.3, which is the typical value for most solids, the numerical data by Wu et al. for a 20-μm sphere colliding with a flat substrate are used to fit the impulse ratio. Figure 2 shows the numerical data on impulse ratio for collisions between an elastic sphere and an elastic substrate (elastic-elastic (EE) collision) and collisions between an elastoplastic sphere and an elastic substrate (plastic-elastic (PE) collision). The fitted curve shown in Figure 2 is given by the following equation

$$f/\mu = \begin{cases} -0.0074\psi^3 + 0.0563\psi^2 + 0.094\psi & 0 < \psi < \psi_{\text{crit}} \\ 1 & \psi \ge \psi_{\text{crit}} \end{cases} \tag{21}$$

where ψ is the normalized angle at the contact patch, defined by $\psi = 2\tan\theta_{ci}/(1+e_n)\mu$ with θ_{ci} the incident angle of the contact

patch. The critical normalized impact angle, ψ_{crit}, beyond which the sliding occurs throughout contact is given by

$$\psi_{\text{crit}} = (7\kappa - 1)/\kappa \tag{22}$$

where κ represents the ratio of initial tangential contact stiffness to the normal contact stiffness calculated from Poisson's ratio, v, and is given by

$$\kappa = \frac{2(1-v)}{2-v} \tag{23}$$

Equation 21 differs from the expression used by Wu et al.[26] but yields similar accuracy. A polynomial expression is used here instead of the hyperbolic tangent function to facilitate the integration when deriving the boundary conditions for granular flows. The current correlation agrees with the experimental data and FEA results in the literature.[26]

By knowing the impulse ratio, the complete rebound kinematics can be obtained. For example, we can get

$$e_{\text{t}} = 1 - \text{sign}(\psi)(f/\mu)(1+e_{\text{n}})\mu\cot\theta_{\text{i}} \tag{24}$$

$$\Psi_{cr} = \psi - 7\text{sign}(\psi)(f/\mu) \tag{25}$$

where Ψ_{cx} is the dimensionless rebound tangential surface velocity at the contact patch introduced by Wu et al.[26] as

$$\Psi_{cr} = \frac{2\tilde{c}_{\text{t,r}}}{(1+e_{\text{n}})\mu c_{\text{n,i}}} \tag{26}$$

Wu et al.[26] indicated that the semi-analytical model works reasonably well for the particle-wall impact with initial in-plane spin. To extend Eq. 21 for $\psi < 0$, which is usually encountered in collisions with initial spin, f/μ is assumed to be an even function of ψ because the contact forces depend on the relative velocity at the contact surfaces. Consequently, Ψ_{cx} must be an odd function of ψ for an oblique impact with initial spin. Figure 3 presents the numerical data of DEM simulations on oblique impacts of a sphere with a plane surface with different initial angular velocities in terms of normalized impact parameters ψ and Ψ_{cx}.[29] Data sets for oblique impacts with different initial angular velocities collapse into one master curve showing a rotational symmetry with respect to 0. The curve based on Eq. 25 by using Eq. 21 for f/μ is superimposed in Figure 3. The agreement between the curve and the numerical data of the discrete element method (DEM) simulation confirms the applicability of the model of Wu et al. for particle-wall impacts with initial in-plane spin.

Effect of Particle Spin

In granular flows, angular velocity of the particle is not zero due to shearing effect and oblique inter-particle and particle-wall collisions. However, not many experimental data are available in the open literature for oblique collisions between a sphere and a flat surface with initial spin. Dong and Moys[12] measured collisions between a 44.5-mm steel ball and a steel flat surface with and without initial spin. Results on normal and tangential restitution coefficients, impulse ratio, angular velocity, and rebound angle of the contact point were reported. They demonstrated that the collision with pre-impact spin did not comply with the model by Maw et al.[30] Similarly, Thornton[31] concluded that the normalized impact parameters of Maw et al.[30,32] were not appropriate for oblique impacts with initial particle spin. Both rigid-body analysis (Eq. 20) and the model of Wu et al. (Eq. 24) indicate that the initial spin of the particle affects the tangential momentum exchange. The pre-collision angular velocity alters when and in which direction the sliding takes place. Figure 4 presents variations of the tangential restitution coefficient with the impact angle with and without initial spin predicted by the rigid-body theory and the model of Wu et al. For a particle with zero initial spin as shown in Figure 4(a), the tangential restitution coefficient becomes a constant of 5/7, according to the rigid-body theory. However, many studies have shown that the tangential restitution coefficient varies with the impact angle for non-sliding collisions. With this respect, the model by Wu et al. predicts more realistic results, which are consistent with experimental measurements. For impacts with spin before collision in Figure 4(b), both models predict similar trends of the tangential restitution coefficient. In Figure 4, the critical impact angles indicating the transition between sliding and nonsliding are shown for different angular velocities. Compared to impacts with zero initial spin, the precollision angular velocity affects the post-collision kinematics profoundly in the nonsliding regime. In the sliding regime, the initial spin does not affect the tangential restitution coefficient.

Figure 5 compares Eqs. 20 and 24 to experimental measurements on the tangential restitution coefficient of oblique impacts of a sphere with initial spin by Dong and Moys.[12] For the 44.5-mm steel ball dropped onto an inclined steel surface with a forward initial spin of about 80 rad/s, the ball slides at the contact point throughout. Both equations predict an identical profile. Agreement between the experimental measurements and predictions is shown in Figure 5(a). For low-impact angles, the incident and rebounded traces of particles are on the same side of the normal line of the contact surface, leading to a negative tangential restitution coefficient which cannot be observed for the impact with zero initial spin. In Figure 5(b), the backward initial spin hinders sliding of the contact point, so the nonsliding collision usually occurs. For collisions with small impact angles, the tangential restitution coefficient exceeds the unit and increases as the impact angles decrease, because of the initial spin. Again, both the rigid-body theory and the model of Wu et al. predict this trend reasonably well, though both equations slightly overpredict the tangential restitution coefficients. It should be noted that we only consider an in-plane spin in our current analysis. Impact with an arbitrary angular velocity is more complicated and beyond the scope of this study.

Revisiting Johnson and Jackson Boundary Condition

Johnson and Jackson[14] developed the boundary conditions for granular flows by equating the tangential force per unit area exerted on the boundary by the flowing particles to the corresponding stress within the particles flow approaching the boundary. The force exerted on the boundary by particles is the sum of collisional and frictional contributions during collisions. Hence, the following condition is derived for the slip velocity at the wall.

$$\frac{\mathbf{u}_{\text{sl}}\cdot(\boldsymbol{\sigma}_{\text{c}}+\boldsymbol{\sigma}_{\text{f}})\cdot\mathbf{n}}{|\mathbf{u}_{\text{sl}}|} + \frac{\phi\sqrt{3\Theta}\pi\rho_{\text{p}}\alpha_{\text{p}}|\mathbf{u}_{\text{sl}}|}{6\alpha_{\text{p,max}}\left[1-(\alpha_{\text{p}}/\alpha_{\text{p,max}})^{1/3}\right]} + N_{\text{f}}\tan\delta = 0 \tag{27}$$

The first term on the left side of Eq. 27 denotes the stress in the solids flow on approaching the wall. Here, $\mathbf{u}_{\text{sl}}$ is the

slip velocity between the particles and the wall, $\boldsymbol{\sigma}_c$ and $\boldsymbol{\sigma}_f$ are collisional and frictional stress tensors, respectively, and $\mathbf{n}$ is the unit normal vector of the wall. The second term stands for the rate of tangential momentum transfer to the wall by particle-wall collisions, which is the product of the collision frequency for each particle, $\sqrt{3\Theta}/s$, the average tangential momentum transferred per collision, $\phi\rho_p\pi d_p^3\mathbf{u}_{sl}/6$, and the number of particles adjacent to unit area of the wall, $1/a_c$. Here, s denotes the average distance between the wall and an adjacent particle, estimated by $s = d_p[(\alpha_{p,max}/\alpha_p)^{1/3} - 1]$, a_c is the average boundary area per particle read as $a_c = d_p^2(\alpha_{p,max}/\alpha_p)^{2/3}$, and ϕ is the specularity coefficient. ρ_p is the density of the solid material, d_p is the particle diameter, Θ is the granular temperature, α_p is the solid's volume fraction, and $\alpha_{p,max}$ is the solid's volume fraction at a closely random packing state. The third term on the left side of Eq. 27 is the stress due to sliding particles, which is obtained by applying Coulomb's law of friction to the particles sliding over the surface. N_f is the normal frictional component of stress, that is, the frictional pressure, and δ is the angle of friction between the surface and the particles.

For the fluctuation energy (or granular energy), Johnson and Jackson[14] derived the following boundary condition

$$-\mathbf{n}\cdot\mathbf{q}_{PT} = D + \mathbf{u}_{sl}\cdot\mathbf{S}_c^b \tag{28}$$

where $\mathbf{q}_{PT}$ is the flux of fluctuation energy and D is the rate of dissipation of fluctuation energy due to inelastic particle-wall collisions expressed as

$$D = \frac{1}{4}\pi\rho_p d_p^3\Theta(1-e_w^2)\frac{\sqrt{3\Theta}}{d_p\left[(\alpha_{p,max}/\alpha_p)^{1/3}-1\right]}\frac{1}{d_p^2(\alpha_{p,max}/\alpha_p)^{2/3}} \tag{29}$$

where e_w is the normal restitution coefficient of particle-wall collisions, which is equivalent to e_n in the previous analyses for single particle-wall collision. $\mathbf{S}_b^c$ is the force per unit area on the wall due to particle-wall collisions given by

$$\mathbf{S}_c^b = \frac{\phi\sqrt{3\Theta}\pi\rho_p\alpha_p|\mathbf{u}_{sl}|}{6\alpha_{p,max}\left[1-(\alpha_p/\alpha_{p,max})^{1/3}\right]} \tag{30}$$

In most numerical simulations, an *ad hoc* patching approach suggested by Savage[33] is used to unify the available models for the rapid flow regime dominated by the interparticle collision and the quasi-static regime dominated by the surface friction. Frictional stress comes into play only at high solids concentration, usually about 0.5. For this reason, the below equation is commonly used for the slip velocity together with Eq. 28 for granular energy at the wall.

$$\frac{\mathbf{u}_{sl}\cdot\boldsymbol{\sigma}_c\cdot\mathbf{n}}{|\mathbf{u}_{sl}|} + \frac{\phi\sqrt{3\Theta}\pi\rho_p\alpha_p|\mathbf{u}_{sl}|}{6\alpha_{p,max}\left[1-(\alpha_p/\alpha_{p,max})^{1/3}\right]} = 0 \tag{31}$$

Interpretation of Specularity Coefficient

In the above boundary conditions, the specularity coefficient ϕ is defined to be the average fraction of relative tangential momentum transferred in a particle-boundary collision. The specularity coefficient was first introduced by Hui et al.[15] to measure the fraction of collisions that transfer a significant amount of lateral momentum to the wall. With this parameter, the average tangential momentum transferred per collision is written as

$$\overline{M}_{t,w} = \phi\rho_p\pi d_p^3 u_{sl}\Big/6 \tag{32}$$

According to Johnson and Jackson,[14] its value depends on the large-scale roughness of the surface and varies between zero for perfectly specular collisions and unity for perfectly diffuse collisions. For large-scale roughness with the wavelength and amplitude comparable to the particle size, ϕ will be large. To obtain the value of ϕ, Hui et al.[15] recommended that the tangential velocity changes should be measured for a large number of collisions with different impact velocities and impact angles on a representative section of the wall. However, no such measurement has been reported in the literature. In addition, it will be demonstrated that the specularity coefficient is closely related to both the flow conditions and the wall properties and cannot be determined independently.

For a flat, frictional wall, the measurement suggested by Hui et al.[15] can be done numerically by assuming certain particle velocity distribution close to the wall. The tangential momentum transferred to a frictional flat surface due to the particle-wall collision can be expressed as

$$\mathbf{M}_{t,w} = (1-e_t)\rho_p\pi d_p^3\mathbf{c}_{t,i}/6 \tag{33}$$

Assuming in-plane rotation of the particle, we can calculate the tangential momentum transfer based on the rigid-body analysis as

$$\mathbf{M}_{t,w} = \begin{cases} \frac{\rho_p\pi d_p^3}{21}\left(c_{t,i}-R\omega_i\right)\mathbf{t} & \left|c_{t,i}-R\omega_i\right| \le \frac{7}{2}\mu(1+e_n)c_{n,i} \\ \mathrm{sign}(c_{t,i}-R\omega_i)\frac{\rho_p\pi d_p^3\mu(1+e_n)c_{n,i}}{6}\mathbf{t} & \text{otherwise} \end{cases} \tag{34}$$

To obtain the final form of the mean momentum transferred to the wall due to collisions, an appropriate particle velocity distribution function for granular flows in the near wall region is needed to conduct the integration as discussed by Jenkins.[5] According to the kinetic theory, the frequency distribution of velocities $f(t, \mathbf{r}, \mathbf{c})$ of particles is a function of time t, position $\mathbf{r}$, and instantaneous velocity $\mathbf{c}$. The average value $<\zeta>$ of a quantity ζ is defined to be

$$<\zeta> = \frac{1}{N}\int\zeta f(t,\mathbf{r},\mathbf{c})d\mathbf{c} \tag{35}$$

where N is the number of particles per unit volume at t and $\mathbf{r}$. Similar to Jenkins and Louge,[6] the isotropic Maxwellian distribution is used, noting that it has been shown the leading-order distribution for gravity-driven Poiseuille granular flow.[34] The isotropic Maxwellian velocity distribution used to carry out the average is

$$f(t,\mathbf{r},\mathbf{c}) = \frac{N}{(2\pi\Theta)^{3/2}}\exp\left(-\frac{(\mathbf{c}-\mathbf{u})^2}{2\Theta}\right) \tag{36}$$

where $\mathbf{u}$ is the mean velocity of particles. The granular temperature Θ, which describes the kinetic energy associated with the particle fluctuation, is defined as

$$\Theta = \frac{1}{3}<(\mathbf{c}-\mathbf{u})^2> \tag{37}$$

Equation 36 can be written as

$$f(\mathbf{C}^2)=\frac{N}{(2\pi\Theta)^{3/2}}\exp\left(-\frac{\mathbf{C}^2}{2\Theta}\right)=NF(C_x)F\left(C_y\right)F(C_z) \quad (38)$$

where $\mathbf{C}=\mathbf{c}-\mathbf{u}$, $C^2=C_x^2+C_y^2+C_z^2$ and $F(C)=\frac{1}{(2\pi\Theta)^{1/2}}\exp(\frac{-C^2}{2\Theta})$. The deviation of velocity distribution function from the Maxwellian distribution has been generally acknowledged and extensively studied through theory, simulation, and experiment for a driven granular flow. Unfortunately, the form of the velocity distribution function differs, and it remains an open question.[35,36] Therefore, the Maxwellian distribution function is adopted in the following analysis.

The mean particle flow is treated as two-dimensional, with x and y representing directions normal to the wall and along the flow. Limited by the previous analysis on single particle-wall collision, the mean particle angular velocity ω is in z direction only, with z being the third dimension normal to the $x-y$ plane. Further ignoring the fluctuation in angular velocity, the mean tangential momentum transferred to a frictional flat surface can be calculated as

$$\bar{M}_{\mathrm{t,w}}=\int F(\mathbf{C}^2)\mathbf{M}_{\mathbf{t,w}}d\mathbf{C}=\frac{1}{N}\frac{\rho_{\mathrm{p}}\pi d_{\mathrm{p}}^3}{21}\int_0^\infty\int_{-\infty}^{\infty}\int_{-\infty}^{\infty}f\left(\mathbf{C}^2\right)$$
$$\begin{cases}\left(u_{\mathrm{sl}}-R\omega+C_y\right) & \left|\sqrt{\left(u_{sl}-R\omega+C_y\right)^2+C_z^2}\right|\le\frac{7}{2}\mu(1+e_n)C_x\\ \mathrm{sign}\left(u_{sl}-R\omega+C_y\right)\frac{7\mu(1+e_{\mathrm{n}})}{2}C_x & \text{otherwise}\end{cases}$$
$$\times dC_zdC_ydC_x \quad (39)$$

Introducing $k=\frac{7}{2}\mu(1+e_n)$, $u=u_{sl}-R\omega$ with ω denoting the mean angular velocity and an approximation of $\sqrt{(u_{sl}-R\omega+C_y)^2+C_z^2}\approx|u_{sl}-R\omega+C_y|$, Eq. 39 can be expanded as

$$\bar{M}_{t,w}=\frac{\rho_{\mathrm{p}}\pi d_{\mathrm{p}}^3}{21}\int_0^\infty\left(\int_{-kC_x-u}^{kC_x-u}(u+C_y)F\left(C_y\right)dC_y+\int_{-\infty}^{-kC_x-u}\right.$$
$$\left.-kC_xF\left(C_y\right)dC_y+\int_{kC_x-u}^{\infty}kC_xF\left(C_y\right)dC_y\right)F(C_x)dC_x$$
$$=\underbrace{\frac{\rho_{\mathrm{p}}\pi d_{\mathrm{p}}^3}{21}\int_0^\infty F(C_x)\frac{1}{2}u\left(\mathrm{erf}(\frac{-u+kC_x}{\sqrt{2}\sqrt{\Theta}})+\mathrm{erf}(\frac{u+kC_x}{\sqrt{2}\sqrt{\Theta}})\right)dC_x}_{\mathrm{I}}$$
$$+\underbrace{\frac{\rho_{\mathrm{p}}\pi d_{\mathrm{p}}^3}{21}\int_0^\infty F(C_x)\frac{\sqrt{\Theta}}{\sqrt{2\pi}}\left(-\exp(-\frac{(u-kC_x)^2}{2\Theta})\right.}_{\mathrm{II}}$$
$$\left.+\exp(-\frac{(u+kC_x)^2}{2\Theta})\right)dC_x$$
$$+\underbrace{\frac{\rho_{\mathrm{p}}\pi d_{\mathrm{p}}^3}{21}\int_0^\infty F(C_x)\frac{1}{2}kC_x\left(\mathrm{erf}(\frac{u-kC_x}{\sqrt{2}\sqrt{\Theta}})-\mathrm{erf}(\frac{u+kC_x}{\sqrt{2}\sqrt{\Theta}})\right)dC_x}_{\mathrm{III}} \quad (40)$$

An effective specularity coefficient, ϕ', can be calculated as

$$\phi'=6\bar{M}_{\mathrm{t,w}}\Big/\rho_p\pi d_p^3u \quad (41)$$

Unfortunately, we are only able to derive an approximated analytical expression for the effective specularity coefficient from the above integration for $k<1$ as outlined in Appendix A. The effective specularity coefficient is a function of k and r only, with $r=u/\sqrt{3\Theta}$, a normalized slip velocity at the wall characterizing the mean impact angle of particles. The same conclusion can be obtained for $k\ge1$, where we have to rely on the numerical integration. A similar procedure can be applied to the tangential restitution coefficient derived based on the model of Wu et al. given in Eq. 24, which yields a similar result with slightly quantitative differences. Because k is dependent on both e_{n} and μ, Figure 6 compares the effective specularity coefficients predicted by both models for different particle-wall restitution coefficients and frictional coefficients. For comparison, the effective specularity coefficients predicted by assuming all collisions are sliding or non-sliding are shown in the figure as dashed lines.

As shown in Figure 6, the effective specularity coefficient increases as the normal particle-wall restitution coefficient and the wall frictional coefficient increase. For large r with high normalized slip velocity, the effective specularity coefficient is identical to the all-sliding approximation. For low values of r, most collisions are nonsliding, and the effective specularity coefficient approaches the limit of 1/7 predicted by the non-sliding assumption according to the rigid-body theory as the frictional coefficient increases. The predictions based on the model of Wu et al. are very similar to that by the rigid-body theory, with the difference mainly at low values of r. The difference between them increases with the frictional coefficient and the restitution coefficient. Overall, the difference is less than 20% for $\mu<1$, encountered in most applications. In addition, Figure 6 indicates that the effective specularity coefficient is more sensitive to the frictional coefficient than the normal particle-wall restitution coefficient.

For a given problem with a specified normal particle-wall restitution coefficient and frictional coefficient, the dependence of the effective specularity coefficient on flow behavior can be obtained through numerical integration. Alternatively, the following analytical expression based on the rigid-body theory can be used for low particle-wall friction with $k<1$.

$$\phi'=\frac{1}{105\sqrt{3}\pi^{3/2}r}\left\{2\exp(-\frac{3r^2}{2})k\sqrt{3\pi}r(15+5k^2(-4+3r^2)\right.$$
$$+3k^4(6-11r^2+3r^4))+15\sqrt{2}\pi\left(\mathrm{erf}\left(\sqrt{\frac{3}{2}}r\right)k\right.$$
$$\left.\left.-\frac{1}{\sqrt{1+k^2}}\exp\left(-\frac{3\mathrm{r}^2}{2+2\mathrm{k}^2}\right)\mathrm{erf}\left(\frac{1}{\sqrt{1+\mathrm{k}^2}}\sqrt{\frac{3}{2}}\mathrm{kr}\right)\right)\right\} \quad (42)$$

Unfortunately, k is greater than the unit in most circumstances. A working expression can be obtained by simply fitting the numerical integration data based on the rigid-body theory.

$$\phi'=\begin{cases}-\frac{7\sqrt{6\pi}\left(\phi_0'\right)^2}{8k}r+\phi_0' & r\le\frac{4k}{7\sqrt{6\pi}\phi_0'}\\ \frac{2}{7}\frac{k}{r\sqrt{6\pi}} & \text{otherwise}\end{cases} \quad (43)$$

where ϕ_0' is the value of ϕ' when r goes to zero, which can be approximated through the numerical integration by setting a small value for r. Figure 7 shows the variation of the effective specularity coefficient based on the rigid-body theory, with k for $r = 0.01$, 0.001, and 0.0001. It can be seen from the figure that all curves collapse into one single line which can be used to approximate ϕ_0'. For the range of $k\epsilon(0, 10)$ of practical interest, an equation for approximation of ϕ_0' is obtained by curve fitting.

$$\phi_0' = -0.0012596 + 0.1064551k - 0.04281476k^2 + 0.0097594k^3 - 0.0012508258k^4 + 0.0000836983k^5 - 0.00000226955k^6 \quad (44)$$

By using the approximation of ϕ_0' given in Eq. 44, the fitted curves of the effective specularity coefficient based on Eq. 43 are compared against the data through numerical integration in Figure 8. The simple fitted curves show good accuracy for the range of k of practical interest. It is recommended that Eq. 43 should be used instead of Eq. 42 for most granular flow simulations.

To get the final value of specularity coefficient for the Johnson and Jackson's boundary conditions, we have to introduce some assumptions on the mean angular velocity of the particles. Unfortunately, little knowledge has been obtained on particle rotations in granular flows. One can simply ignore the angular velocity of particles so that the specularity coefficient equals the effective specularity coefficient. Alternatively, the mean angular velocity of the spheres can be assumed equal to the angular velocity of the mean flow.[5]

$$\omega = \frac{1}{2}\frac{\partial u_{\mathrm{sl}}}{\partial n} \quad (45)$$

This is only a rough assumption, as no more appropriate theory is available for predicting the mean spin of particles at the boundary,[37] noting that particles can spin due to oblique collisions. Then the specularity coefficient is read as

$$\phi = \left(1 - \frac{R}{2u_{\mathrm{sl}}}\frac{\partial u_{\mathrm{sl}}}{\partial n}\right)\phi' \quad (46)$$

The previous analysis gives the expression for the specularity coefficient, which can be used in Johnson and Jackson's boundary conditions for a flat wall without an explicit consideration of the wall roughness. However, the boundary condition should account for the wall roughness, as it considerably alters the collision process and the collision frequency.[25] A stochastic approach was developed to include the wall roughness effect on wall collisions in the Lagrangian modeling of particle flows.[25,38] In that model, the wall roughness is accounted by assuming that the impact angle is composed of the trajectory angle with respect to the plane wall and a stochastic component caused by the wall roughness. However, it is difficult to incorporate such a model into the boundary conditions for two-fluid model, as the individual collisional angle is not tracked. On the other hand, the frictional coefficient is a material property dependent on the surface properties, including asperities and roughness. Hence, the small-scale roughness can be included in the frictional coefficient measured in experiments, for example, with the method outlined by Li et al.[39] This is considered reasonably accurate for a surface with well-controlled roughness. For large-scale roughness, one might use the boundary conditions developed for a bumpy boundary[7,9] or simply use a large value for ϕ. During the derivation of expression for the specularity coefficient, we focus only on the momentum transfer between particles and the wall. Hence, its accuracy when apply to the boundary condition for the fluctuation energy needs further investigation, which will be addressed in future studies.

Comparison with Jenkins' theory and Louge's data

It should be noted that no previous measurement or analysis was reported on the specularity coefficient. To verify the above analysis, the ratio between the magnitudes N and S of the normal and tangential components of the force per unit area applied by the granular flow to the wall is compared with the previous study by Jenkins[5] as well as the numerical results from particle simulations by Louge.[37]

Jenkins[5] derived the boundary conditions at a flat, frictional wall based upon a model of collision that distinguishes between sticking and sliding collisions. He obtained analytical expressions for collisional exchange of momentum and fluctuation energy between particles and the wall in two asymptotic circumstances—the small-friction/all-sliding limit and the large-friction/no-sliding limit. In the small-frication/all sliding limit, the ratio of shear stress S to the normal stress N is

$$S/N = \mu \quad (47)$$

In the large-friction/no-sliding limit, the ratio is

$$S/N = \frac{3}{7}\frac{1+\beta_0}{1+e_{\mathrm{n}}}r \quad (48)$$

where $0 \le \beta_0 \le 1$ is the tangential restitution coefficient based on precollision and postcollision velocity at the contact point.

Louge[37] used computer simulations to test Jenkins's theory for the interaction between a rapid granular flow and a flat, frictional wall. Detailed numerical data on the flow-wall interaction were reported over a wide range of collisional properties for the wall and the flow particles. Figure 9 compares the stress ratios predicted by the current study with those of Jenkins's theory and Louge's particle simulations. For convenience, the plots are shown in the form of a normalized stress ratio, $\mathbf{R} = \frac{7}{2}\frac{1+e_n}{1+\beta_0}\frac{S}{N}$. This study shows reasonable consistency with Jenkins' theory and Louge's data. Predictions based on both rigid-body analysis and model of Wu et al. agree with the data of particle simulations for large values of r. For small normalized slip velocities, the difference between the current study and Louge's data can be caused by different reasons, including isotropic assumption on granular temperature, ignorance of spin temperature, and the simple Maxwellian velocity distribution used in the analysis. It should be noted that better agreement between rigid-body analysis and Louge's data rather than the model of Wu et al. is due to the fact that the hard-sphere discrete particle simulations were conducted with a simple particle-wall collision model, which is essentially the rigid-body theory when $\beta_0 = 0$. However, the results based on the model of Wu et al. are considered more accurate, as the rigid-body theory fails to include the tangential, elastic compliance of the contact surfaces, provided a proper velocity distribution function is used. Toward this end, soft-sphere DEM simulations with accurate physical models on the particle-wall interaction are needed for the development

of appropriate particle velocity distribution and verification of the current study.

Summary and Conclusions

In this work, we revisit the boundary conditions for granular flows developed by Johnson and Jackson.[14] By adopting the classic rigid-body theory and the more realistic model of Wu et al. for the particle-wall collision, dependence of the specularity coefficient on properties of particle-wall collision and flow behavior is determined by using the isotropic Maxwellian velocity distribution. Only the normal particle-wall restitution coefficient and wall frictional coefficient are needed as inputs for the Johnson and Jackson boundary conditions. An analytical expression for the specularity coefficient is suggested for a flat, frictional surface with a low frictional coefficient. A working expression for the specularity coefficient is provided for a general problem based on the numerical integration.

Acknowledgments

This technical effort was performed in support of the National Energy Technology Laboratory's ongoing research in advanced multiphase flow simulation under the RES contract DE-FE0004000. The authors acknowledge helpful comments provided by Drs. Madhava Syamlal, Thomas O'Brien, and N'dri Arthur Konan.

Notation

$\mathbf{c}$ = translational velocity
$\mathbf{C}$ = fluctuating velocity
d = diameter
e = restitution coefficient
f = impulse ratio
I = moment of inertia
$\mathbf{J}$ = impulse
$k = \frac{7}{2}\mu(1+e_{\mathrm{n}})$
m = mass of particle
$\mathbf{M}$ = momentum
$\mathbf{n}$ = normal wall vector
$\mathbf{N}$ = particle number density or normal stress
$\mathbf{q}$ = flux
r = normalized slip velocity
$\mathbf{r}$ = position
R = particle radius
$\mathbf{R} = \frac{7}{2}\frac{1+e_n}{1+\beta_0}\frac{S}{N}$
S = shear stress
t = time
$\mathbf{t}$ = tangential wall vector
$\mathbf{u}$ = velocity

Greek symbols

α = volume fraction
β_0 = tangential restitution coefficient at contact point
$\boldsymbol{\sigma}$ = stress tensor
ϕ = specularity coefficient
ϕ' = effective specularity coefficient
ψ = normalized impact angle
ν = Poisson's ratio
ρ = density
μ = frictional coefficient
θ = impact angle
Θ = granular temperature
$\boldsymbol{\omega}$ = mean angular velocity
$\boldsymbol{\omega}$ = angular velocity

Subscripts

i = incident
n = normal component
r = reflective or rotational
p = particle
t = tangential component
w = wall

Literature Cited

1. Gidaspow D. *Multiphase Flow and Fluidization: Continuum and Kinetic Theory Descriptions*. Boston: Academic Press, 1994.
2. Jenkins JT, Richman MW. Boundary conditions for plane flows of smooth nearly elastic, circular disks. *J Fluid Mech*. 1986;171:53–69.
3. Pasquarell GC, Ackermann NL. Boundary conditions for planar granular flows. *J Eng Mech*. 1989;115:1283–1302.
4. Richman MW. Boundary conditions based upon a modified Maxwellian velocity distribution for flows of identical, smooth, nearly elastic spheres. *Acta Mech*. 1988;75:227–240.
5. Jenkins JT. Boundary conditions for rapid granular flows: flat, frictional walls. *J Appl Mech*. 1992;59:120–127.
6. Jenkins JT, Louge MY. On the flux of fluctuation energy in a collisional grain flow at a flat, frictional wall. *Phys Fluids*. 1997;9:2835–2840.
7. Jenkins JT. *Boundary conditions for collisional grain flows at bumpy, frictional walls*. In: Poschel T, Luding S, editors. *Lecture Notes in Physics* Berlin and Heidelberg: Springer 2001:125–139.
8. Xu H. *Collisional Granular Flows With and Without Gas Interactions in Microgravity*. Cornell University, Ithaca, 2003.
9. Xu H, Louge M, Reeves A. Solutions of the kinetic theory for bounded collisional granular flows. *Continuum Mech Thermodyn*. 2003;15:321–349.
10. Kharaz AH, Gorham DA, Salman AD. An experimental study of the elastic rebound of spheres. *Powder Technol*. 2001;120:281–291.
11. Gorham DA, Kharaz AH. The measurement of particle rebound characteristics. *Powder Technol*. 2000;112:193–202.
12. Dong H, Moys MH. Measurement of impact behavior between balls and walls in grinding mills. *Miner Eng*. 2003;16:543–550.
13. Benyahia S, Syamlal M, O'Brien TJ. Evaluation of boundary conditions used to model dilute, turbulent gas/solids flows in a pipe. *Powder Technol*. 2005;156:62–72.
14. Johnson PC, Jackson R. Frictional collisional constitutive relations for antigranulocytes-materials, with application to plane shearing. *J Fluid Mech*. 1987;176:67–93.
15. Hui K, Haff PK, Ungar JE. Boundary conditions for high-shear grain flows. *J Fluid Mech*. 1984;145:223–233.
16. Li T, Grace JR, Bi X. Study of wall boundary condition in numerical simulations of 2D bubbling fluidized beds. *Powder Technol*. 2010;203:447–457.
17. Li T, Zhang Y, Grace JR, Bi X. Numerical investigation of gas mixing in gas-solid fluidized beds. *AIChE J*. 2010;56:2280–2296.
18. Jin B, Wang X, Zhong W, Tao H, Ren B, Xiao R. Modeling on high-flux circulating fluidized bed with Geldart group B particles by kinetic theory of granular flow. *Energy Fuels*. 2010;24:3159–3172.
19. Wang X, Jin B, Zhong W, Xiao R. Modeling on the hydrodynamics of a high-flux circulating fluidized bed with Geldart group A particles by kinetic theory of granular flow. *Energy Fuels*. 2010;24:1242–1259.
20. Iwashita K, Oda M. Rolling resistance at contacts in simulation of shear band development by DEM. *J Eng Mech*. 1998;124:285–292.
21. Orlando AD, Shen HH. Effect of rolling frication on binary collisions of spheres. *Phys Fluids*. 2010;22:033304.
22. Foerster SF, Louge MY, Chang H, Allia K. Measurements of the collision properties of small spheres. *Phys Fluids*. 1994;6: 1108–1115.
23. Hussainova I, Kubarsepp J, Shcheglov I. Investigation of impact of solid particles against hardmetal and cermet targets. *Tribol Int*. 1999;32:337–344.
24. Labous L, Rosato AD, Dave RN. Measurements of collisional properties of spheres using high-speed video analysis. *Phys Rev E*. 1997;56:5717–5725.
25. Sommerfeld M, Huber N. Experimental analysis and modeling of particle-wall collisions. *Int J Multiphase Flow*. 1999;25:1457–1489.
26. Wu CY, Thornton C, Li LY. A semi-analytical model for oblique impacts of elastoplastic spheres. *Proc R Soc A*. 2009;465:937–960.
27. Di Maio FP, Di Renzo A. Analytical solution for the problem of frictional-elastic collisions of spherical particles using the linear model. *Chem Eng Sci*. 2004;59:3461–3475.
28. Kruggel-Emden H, Wirtz S, Scherer V. An analytical solution of different configurations of the linear viscoelastic normal and frictional-elastic tangential contact model. *Chem Eng Sci*. 2007;62: 6914–6926.
29. Ning Z. *Elasto-Plastic Impact of Fine Particles and Fragmentation of Small Agglomerates*. Birmingham: University of Aston, 1995.
30. Maw N, Barber JR, Fawcett JN. The role of elastic tangential compliance in oblique impact. *J Lubrication Technol*. 1981;103: 74–80.

31. Thornton C. A note on the effect of initial particle spin on the rebound behavior of oblique particle impacts. *Powder Technol*. 2009;192:152–156.
32. Maw N, Barber JR, Fawcett JN. The oblique impact of elastic spheres. *Wear*. 1976;38:101–114.
33. Savage SB. *Granular flow down rough inclines—review and extension*. In: Jenkins JT, Satake M, editors. *Mechanics of Granular Materials: New Model and Constitutive Relations*. New York: Elsevier Science Ltd., 1983:261–282.
34. Alam M, Chikkadi VK. Velocity distribution function and correlations in a granular Poiseuille flow. *J Fluid Mech*. 2010;653:175–219.
35. Losert W, Cooper DGW, Delour J, Kudrolli A, Gollub JP. Velocity statistics in excited granular media. *Chaos*. 1999;9:682.
36. van Zon JS, MacKintosh FC. Velocity distributions in dilute granular systems. *Phys Rev E*. 2005;72:051301.
37. Louge MY. Computer simulations of rapid granular flows of spheres interacting with a flat, frictional boundary. *Phys Fluids*. 1994;6:2253.
38. Sommerfeld M. Modelling of particle/wall collisions in confined gas-particle flows. *Int J Multiphase Flow*. 1992;18:905–926.
39. Li YJ, Xu Y, Thornton C. A comparison of discrete element simulations and experiments for 'sandpiles' composed of spherical particles. *Powder Technol*. 2005;160:219–228.

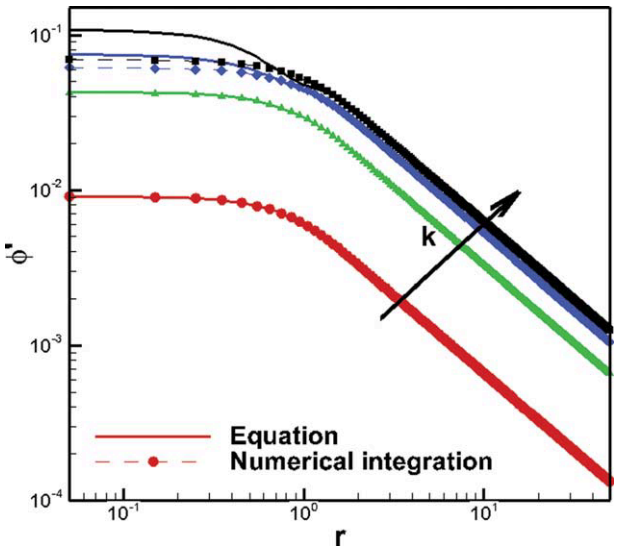

Figure A1. Effective specularity coefficient predicted by the approximated analytical Eq. 53 and numerical integration for k =0.1, 0.5, 0.8, and 0.95.

Appendix A

For part *II* in Eq. 40, we have

$$II = -\frac{\Theta \exp\left(-\frac{u^2}{2\Theta+2k^2\Theta}\right)\mathrm{erf}\left(\frac{ku}{\sqrt{2\Theta+2k^2\Theta}}\right)}{\sqrt{2\pi}\sqrt{(1+k^2)\Theta}} \tag{A1}$$

Unfortunately, no analytical expression can be derived for parts *I* and *III*. One way to do the calculation is to expand the error function with respect to k

$$\begin{aligned} \mathrm{I} \approx \int_0^\infty F(C_x)\frac{1}{2}u\Bigg(&\frac{2\exp\left(-\frac{u^2}{2\Theta}\right)\sqrt{\frac{2}{\pi}}C_x k}{\sqrt{\Theta}} \\ &+\frac{\exp\left(-\frac{u^2}{2\Theta}\right)\sqrt{\frac{2}{\pi}}(u^2-\Theta)C_x^3k^3}{3\Theta^{5/2}} \\ &+\frac{\exp\left(-\frac{u^2}{2\Theta}\right)(u^4-6u^2\Theta+3\Theta^2)C_x^5k^5}{30\sqrt{2\pi}\Theta^{9/2}}\Bigg)dC_x \\ =\exp\left(-\frac{u^2}{2\Theta}\right)&\frac{ku}{\pi}\left(1+\frac{k^2(u^2-\Theta)}{3\Theta}+\frac{k^4(u^4-6u^2\Theta+3\Theta^2)}{15\Theta^2}\right) \end{aligned} \tag{A2}$$

and

$$\begin{aligned} \mathrm{III} \approx \int_0^\infty F(C_x)\frac{1}{2}kC_x\Bigg(&2\mathrm{erf}\left(\frac{u}{\sqrt{2}\sqrt{\Theta}}\right)-\frac{\exp\left(-\frac{u^2}{2\Theta}\right)\sqrt{\frac{2}{\pi}}uC_x^2k^2}{\Theta^{3/2}} \\ &-\frac{\left(\exp\left(-\frac{u^2}{2\Theta}\right)u(u^2-3\Theta)C_x^4\right)k^4}{6\left(\sqrt{2\pi}\Theta^{7/2}\right)}\Bigg)dC_x \\ =\frac{k\sqrt{\Theta}\mathrm{erf}\left(\frac{u}{\sqrt{2}\sqrt{\Theta}}\right)}{\sqrt{2\pi}}&+\frac{\exp\left(-\frac{u^2}{2\Theta}\right)k^3u}{\pi}\left(-1+k^2-\frac{k^2u^2}{3\Theta}\right) \end{aligned} \tag{A3}$$

Finally, we get

$$\begin{aligned} \bar{M}_{t,w} = \frac{\rho_\mathrm{p}\pi d_\mathrm{p}^3}{21}\Bigg\{&\exp\left(-\frac{u^2}{2\Theta}\right)\frac{ku}{\pi}\left(1+\frac{k^2(u^2-\Theta)}{3\Theta}\right. \\ &\left.+\frac{k^4(u^4-6u^2\Theta+3\Theta^2)}{15\Theta^2}\right)-\frac{1}{\sqrt{2\pi}\sqrt{(1+k^2)\Theta}}\Theta \\ &\times\exp\left(-\frac{u^2}{2\Theta+2k^2\Theta}\right)\mathrm{erf}\left(\frac{ku}{\sqrt{2\Theta+2k^2\Theta}}\right) \\ &+\frac{1}{\sqrt{2\pi}}k\sqrt{\Theta}\mathrm{erf}\left(\frac{u}{\sqrt{2}\sqrt{\Theta}}\right)+\frac{1}{\pi}\exp\left(-\frac{u^2}{2\Theta}\right)k^3u \\ &\left(-1+k^2-\frac{k^2u^2}{3\Theta}\right)\Bigg\} \end{aligned} \tag{A4}$$

By introducing $r = u/\sqrt{3\Theta}$, the effective specularity coefficient, $\phi' = 6\bar{M}_{i,w}/\rho_p\pi d_p^3 u$, is only a function of r and k.

$$\begin{aligned} \phi' = \frac{1}{105\sqrt{3}\pi^{3/2}r}\Bigg\{&2\exp\left(-\frac{3r^2}{2}\right)k\sqrt{3\pi}r(15+5k^2(-4+3r^2) \\ &+3k^4(6-11r^2+3r^4))+15\sqrt{2}\pi\left(\mathrm{erf}\left(\sqrt{\frac{3}{2}}r\right)k\right. \\ &\left.-\frac{1}{\sqrt{1+k^2}}\exp\left(-\frac{3r^2}{2+2k^2}\right)\mathrm{erf}\left(\frac{1}{\sqrt{1+k^2}}\sqrt{\frac{3}{2}}kr\right)\right)\Bigg\} \end{aligned} \tag{A5}$$

Equation A5 works reasonably well for $k < 1$ as shown in Figure A1, where the predictive values of the effective specularity coefficient are compared to the numerical integration for different values of k. The deviation of Eq. A5 from the numerical integration is mainly within the range where a non-sliding particle-wall collision usually occurs, and it increases with k. For k close to the unit or $k \geq 1$, that is, where the frictional coefficient exceeds 0.14 for nearly elastic particle-wall collisions, using the fitted curve to predict the effective specularity coefficient is recommended.

Manuscript received Apr. 7, 2011 and revision received June 13, 2011.